STRUCTURAL BIOLOGY

Molecular mechanism of SbmA, a promiscuous transporter exploited by antimicrobial peptides

Dmitry Ghilarov[1†], Satomi Inaba-Inoue[2,3,4†], Piotr Stepien[1†], Feng Qu[2,3], Elizabeth Michalczyk[1‡], Zuzanna Pakosz[1,5‡], Norimichi Nomura[6], Satoshi Ogasawara[6], Graham Charles Walker[7], Sylvie Rebuffat[8], So Iwata[6,9,10], Jonathan Gardiner Heddle[1]*, Konstantinos Beis[2,3]*

Antibiotic metabolites and antimicrobial peptides mediate competition between bacterial species. Many of them hijack inner and outer membrane proteins to enter cells. Sensitivity of enteric bacteria to multiple peptide antibiotics is controlled by the single inner membrane protein SbmA. To establish the molecular mechanism of peptide transport by SbmA and related BacA, we determined their cryo–electron microscopy structures at 3.2 and 6 Å local resolution, respectively. The structures show a previously unknown fold, defining a new class of secondary transporters named SbmA-like peptide transporters. The core domain includes conserved glutamates, which provide a pathway for proton translocation, powering transport. The structures show an outward-open conformation with a large cavity that can accommodate diverse substrates. We propose a molecular mechanism for antibacterial peptide uptake paving the way for creation of narrow-targeted therapeutics.

INTRODUCTION

Bacterial species are under continuous warfare with each other for access to nutrients. To gain an advantage in this struggle, they produce antibacterial compounds that target and kill closely related species. Antimicrobial peptides (AMPs), including nonribosomally synthesized peptides (NRPs) and ribosomally synthesized posttranslationally modified peptides (RiPPs), form a key part of this arsenal, together with polyketide natural products acting as antibiotics. Unlike membrane-targeting AMPs, many NRPs and RiPPs inhibit key enzymes in the cytoplasm, which is essential for cell survival. The *Escherichia coli* inner membrane transporter SbmA (EcSbmA) was found in a genetic screen for sensitivity to the azole-modified RiPP antibiotic microcin B17 (MccB17) (*1*) and subsequently was confirmed as the most important determinant of sensitivity to several structurally unrelated RiPPs from Gram-negative bacteria, including the lasso peptide microcin J25 (MccJ25) (*2*), the azole-modified peptide klebsazolicin (KLB) (*3*), and the NRP-polyketide azole–containing antibiotic bleomycin (*4*). Reliance of all these compounds on a single membrane protein for transport is unexpected, given their different sizes and chemical structures (Fig. 1A). Besides these compounds, SbmA was subsequently found to import a variety of other substrates, including the eukaryotic proline-rich AMP Bac7(1-35) (*5*, *6*), and peptide nucleic acid–peptide conjugates (*7*). While the exact natural function of EcSbmA is not established, it is a virulence factor in a avian pathogenic *E. coli* (APEC) (*8*), while its *Brucella abortus* ortholog (BaBacA) is required for chronic intracellular infection in a mouse model (*9*). EcSbmA is isofunctional with BacA from *Sinorhizobium meliloti* (SmBacA), which is critically required for the chronic intracellular infection of root nodule cells that underlies nitrogen-fixing symbiosis with the legume host by transporting nodule-specific defensin-like cysteine-rich peptides (NCRs) (*10*, *11*, *12*). In summary, peptide internalization by SbmA/BacA is a key component of antibiotic sensitivity, legume symbiosis, and virulence phenotypes. The closest functional and structural homolog of SbmA and BacA is the adenosine triphosphate (ATP)–binding cassette (ABC) transporter Rv1819c from *Mycobacterium tuberculosis* (*13*), but it cannot provide full interchangeable function to the SbmA and BacA transporters (*14*). To establish the molecular mechanism of peptide transport and substrate promiscuity of EcSbmA/SmBacA, we determined the cryo–electron microscopy (cryo-EM) structure of both SbmA and BacA proteins in a lipid bilayer mimetic environment, using proteins reconstituted in nanodiscs (NDs), at 3.2 and 6 Å local resolution, respectively.

RESULTS

Because of the small size of SbmA (45-kDa monomer), we raised antibodies against it to increase its size and facilitate structure determination (fig. S1). One Fab showed a monodisperse peak after purification (designated Fab-S11-1). SbmA-Fab-S11-1 was reconstituted in membrane-scaffold protein 1 D1 (MSP1D1) NDs composed of palmitoleoyl-oleoyl phosphatidylethanolamine (POPE), palmitoleoyl-oleoyl phosphatidylglycerol (POPG), and cardiolipin (CL), in a ratio of 7:2:1, to mimic the *E. coli* bilayer composition (fig. S2). To show that reconstitution into NDs did not alter the function of SbmA, we performed ligand binding studies by microscale thermophoresis (MST), demonstrating that SbmA can bind MccB17, bleomycin, and KLB with the dissociation constant (K_d) of 428 ± 89 nM, 88 ± 14 nM, and 849 ± 196 nM, respectively (Fig. 1B). A twofold symmetrical SbmA-Fab complex, with a characteristic "bunny ears"

[1]Malopolska Centre of Biotechnology, Jagiellonian University, Krakow, Poland. [2]Department of Life Sciences, Imperial College London, Exhibition Road, South Kensington, London SW7 2AZ, UK. [3]Rutherford Appleton Laboratory, Research Complex at Harwell, Didcot, Oxfordshire OX11 0FA, UK. [4]Diffraction and Scattering Division, Japan Synchrotron Radiation Research Institute, SPring-8, 1-1-1, Kouto, Sayo, Hyogo 679-5198, Japan. [5]Postgraduate School of Molecular Medicine, Warsaw, Poland. [6]Department of Cell Biology, Graduate School of Medicine, Kyoto University, Yoshida-Konoe-cho, Sakyo-ku, Kyoto 606-8501, Japan. [7]Department of Biology, Massachusetts Institute of Technology, Cambridge, MA 02139, USA. [8]Molecules of Communication and Adaptation of Microorganisms Laboratory (MCAM, UMR 7245 CNRS-MNHN), Muséum National d'Histoire Naturelle, Sorbonne Universités, Centre National de la Recherche Scientifique, CP 54, 57 rue Cuvier, Paris 75005, France. [9]RIKEN SPring-8 Center, 1-1-1 Kouto, Sayo-cho, Sayo-gun, Hyogo 679-5148, Japan. [10]Research Acceleration Program, Membrane Protein Crystallography Project, Japan Science and Technology Agency, Kyoto, Japan.
*Corresponding author. Email: jonathan.heddle@uj.edu.pl (J.G.H.); kbeis@imperial.ac.uk (K.B.)
†These authors contributed equally to this work.
‡These authors contributed equally to this work and are listed alphabetically.

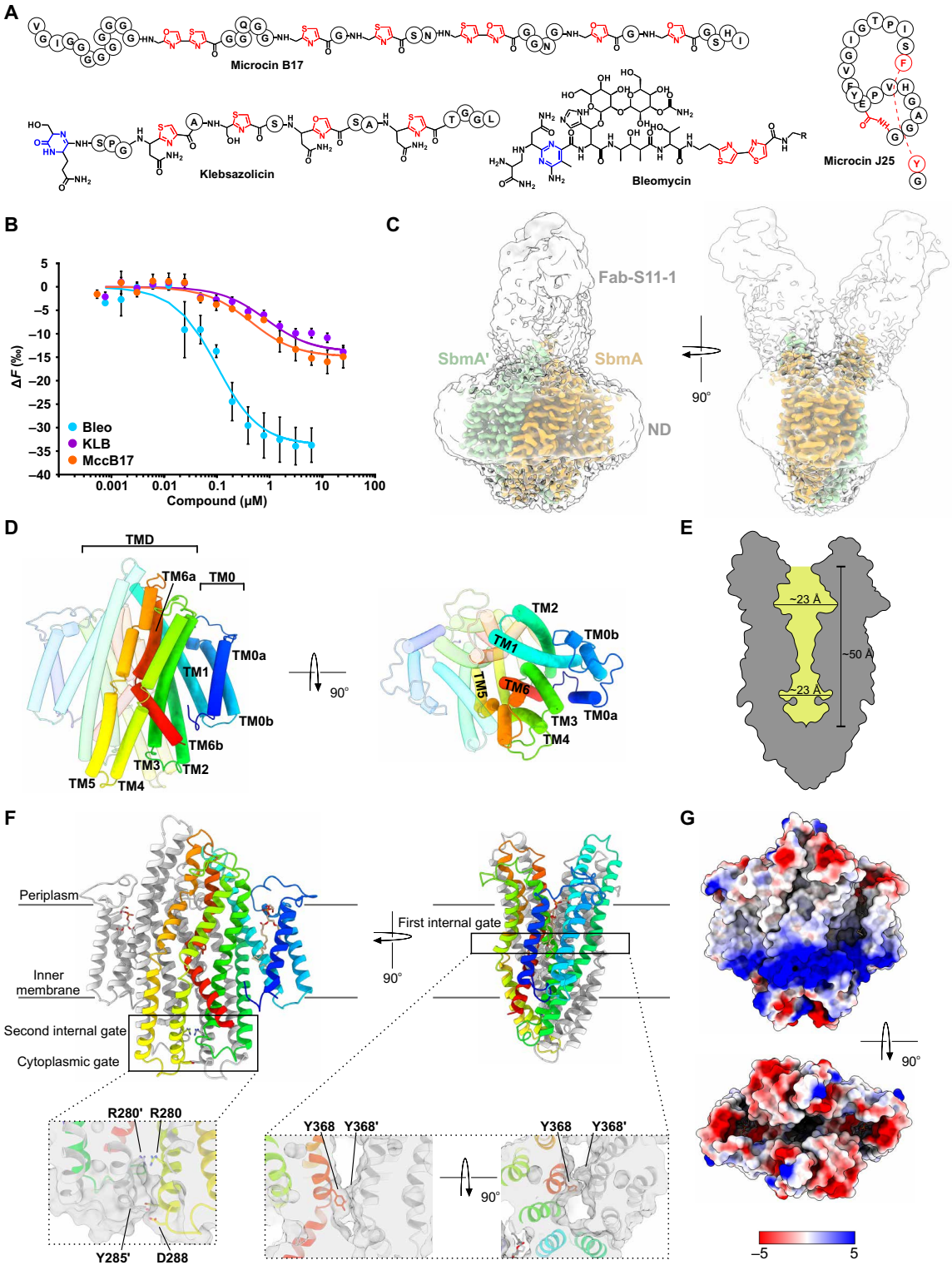

Fig. 1. Structural characterization of SbmA. (**A**) Antibiotic peptide substrates of SbmA. Azoles in MccB17 and KLB are labeled in red; lactamidine and piperidine in KLB and bleomycin, respectively, are in blue; MccJ25 is a cyclic peptide closed by an isopeptide bond (in red) having a threaded topology. Bleomycin sulfate used in this study is a mixture of related compounds containing different C-terminal groups (R). (**B**) MST curves showing binding of MccB17, bleomycin, and KLB to the ND-embedded SbmA. (**C**) EM map of SbmA-FabS11-1-ND complex. Two maps contoured at different levels are overlaid to represent both high-resolution (SbmA) and low-resolution (ND) parts. (**D**) Tube diagram for SbmA. TM helices mentioned in the text are shown. (**E**) A slice through SbmA showing the internal cavity and constriction near Tyr^{368}. Cavity dimensions are indicated. (**F**) A ribbon diagram showing bound PG lipid (stick representation) and gates mentioned in the text. (**G**) Surface representation of SbmA colored by electrostatic potential. Top (red, negative) and bottom (blue, positive) patches are visible.

appearance, was immediately obvious in electron micrographs and two-dimensional (2D) class averages (fig. S3), which agrees with our previous study showing that SbmA exists as a homodimer (*15*). We obtained a 3D reconstruction initially at 3.74 Å global resolution for SbmA-Fab-S11-1-ND, which was subsequently improved to 3.6 Å for the SbmA-Fab-S11-1-MccB17 dataset (see below); the local resolution for SbmA was estimated as 3.2 Å, allowing identification of side chains (Fig. 1A and fig. S3). Continuous Coulomb potential density could be observed for both the SbmA and Fab S11-1, which allowed us to build its de novo structure from residues 1 to 391 (Fig. 1B); no density could be observed for the last 25 residues. Density for the MSP1D1 ND forming a tight belt around the protein was also apparent, defining the section of the protein embedded in the membrane (Fig. 1B). Given the partial flexibility of the Fab fragments (local resolution <6 Å), they have been placed only as rigid molecules and not refined.

SbmA is a homodimer consisting of eight transmembrane (TM) helices per protomer. SbmA consists of two TM0 domains and a core TM domain (TMD), which comprises 12 TM helices; we designated the first two TMs of the TM0 domain as TMs 0a and 0b and the core of the transporter as TMs 1 to 6 (Fig. 1D). The overall structure of TMD notably resembles the TMD of ABC transporters (exporters), such as MsbA (lipid A flippase) (*16*) from *E. coli*, Sav1866 (multidrug resistance) from *Staphylococcus aureus* (*17*), and Rv1819c (cobalamin transporter) from *M. tuberculosis* (fig. S4) (*13*). Despite these similarities, the structural organization of SbmA has not been observed in secondary transporters before; ABC transporter fold refers to full-length ABC transporters containing a nucleotide binding domain (NBD). Therefore, SbmA defines a new fold for secondary transporters, which we named SbmA-like peptide transporter (SLiPT) fold. Rv1819c also contains an additional extended TM helix 0 that interacts with TMs 1 and 2 forming a cap at the periplasmic side of the TMD (*13*), but its overall structure does not display any similarity with the TM0 of SbmA (fig. S4). The SbmA dimer interface is formed between TMs 1 and 2 and 5 and 6 from one protomer and the equivalent ones from the second; TMs 1 and 2 form intermolecular contacts with TMs 5′ and 6′, and TMs 5 and 6 form intermolecular contacts with TMs 1′ and 2′. The TM0 domain of SbmA is a novel feature of SLiPT transporters, which is not present in any other known transporter structure; TMs 0a and 0b do not participate in the dimer formation, and they do not extend beyond the lipid interface. The core domain spans the bilayer and reaches out into both the periplasmic and cytoplasmic space. In our structure, a phosphatidyl glycerol (PG) lipid is found in the interface of TMs 0a/0b and TM1, suggesting a possible role in either transporter conformational changes or stability in the membrane (fig. S5, S10). We have previously shown that PG lipids are important for the transport activity of the MccJ25 ABC exporter McjD (*18*), whereas PE lipids were important for its structural integrity. Therefore, it is likely that the bound PG facilitates substrate transport. SbmA is trapped in an outward-open conformation that more closely resembles the overall conformation of the nucleotide-bound outward-open MsbA (*16*) and Sav1866 (*17*) structures than the nucleotide-bound outward-occluded Rv1819c; SbmA and the TMD of Sav1866 and Rv1819c can be superimposed with a root mean square deviation of 3.4 and 3.5 Å, respectively, over 350 Cα atoms (fig. S4). Another notable feature of SbmA is the absence of the two coupling helices between TMs 2 and 3 and TMs 4 and 5, which are important for transmitting conformational changes between the NBDs and the TMD of ABC exporters (fig. S4). In SbmA, TMs 2 and 3 and TMs 4 and 5 are linked by short loops without any secondary structure. In the TMD, TMs 4 and 5 display a kink in their midpoint in the membrane, whereas TMs 6 are "broken" helices (we refer to them as TMs 6a and 6b) defining an hourglass-shaped funnel (fig. S6), suggesting flexibility and a possible role in conformational changes associated with the transport cycle. Similar broken helices have been reported for the Rv1819c and secondary transporters, for example, the leucine transporter LeuT from *Aquifex aeolicus*, where it has been shown to be important for its transition from outward- to inward-facing conformation (*19*). In its outward-open conformation, SbmA displays a large cavity open on the periplasmic side, where the peptides can bind and be transported to the cytoplasm (Fig. 1E). However, the cavity is open only halfway; the first internal gate formed by Tyr^{368} and $Tyr^{368'}$ at the bottom of TM 6a constricts it at the midpoint between the periplasm and the inner membrane (Fig. 1, E and F). Two further gates are present, which seal the TMD at the cytoplasmic side of the membrane: a cytoplasmic gate, formed by Tyr^{285} and $Asp^{288'}$, and a second internal gate between Arg^{280} and $Arg^{280'}$ (Fig. 1F). The open cavity that SbmA displays is of sufficient size to accommodate the diverse peptides that it transports. A similar sized cavity is seen in the ABC exporter McjD, where one MccJ25 peptide can fit and be transported (*20*, *21*). The electrostatic map of SbmA (Fig. 1G) shows clear negative (top) and positive (bottom) belts around the surface, which could facilitate top-to-bottom transport of positively charged ions by binding them from the surface of the membrane.

Since SbmA adopts a novel fold, we wanted to exclude the possibility that the Fabs or unusually tight encirclement by MSP1D1 induced structural changes. Therefore, we determined the structure of SbmA in the absence of Fabs in larger MSP1E3D1 NDs, which contained more unsaturated lipids [dioleoyl phosphatidylethanolamine (DOPE):POPG:CL; 13:4:1] to increase membrane fluidity (fig. S7). The ~3.8-Å reconstructions display the same overall fold as the SbmA-FabS11-1 complex, suggesting that neither the Fab nor the size and fluidity of the ND influence the conformation of SbmA. Considering the important biological role of BacA in symbiosis, it is important to show that the insights gained from the SbmA structure can be used to interpret the BacA action, especially as the EcSbmA is isofunctional with the SmBacA. As we were able to obtain a 3.9-Å reconstruction of the Fab-free SbmA, we also determined the low-resolution structure of BacA from *S. meliloti* to probe whether it has a similar fold; the two proteins share ~64% sequence identity (fig. S10). The BacA reconstruction displays the same overall fold as SbmA, in either small or large NDs, but because of resolution limitations, we have not built or refined its structure in the reconstructions (Fig. 2A and fig. S8). The functional activity of reconstituted BacA was tested in MST assays, showing that the BacA-ND complex binds bleomycin and MccB17 with a K_d of 19 ± 11 nM and 31 ± 22 nM, respectively (Fig. 2B). The SbmA structure can fit in the BacA map without any structural changes, including the TM0 domain, suggesting that BacA also adopts an outward-open conformation. The BacA structure provides further evidence that SbmA and BacA define a new class of secondary transporters conserved among different bacterial species. Our attempts to capture bleomycin, MccJ25, or MccB17 peptides bound to SbmA or BacA did not yield any density for them; however, the dataset collected in the presence of MccB17 was chosen as the highest resolution one and was used for model building.

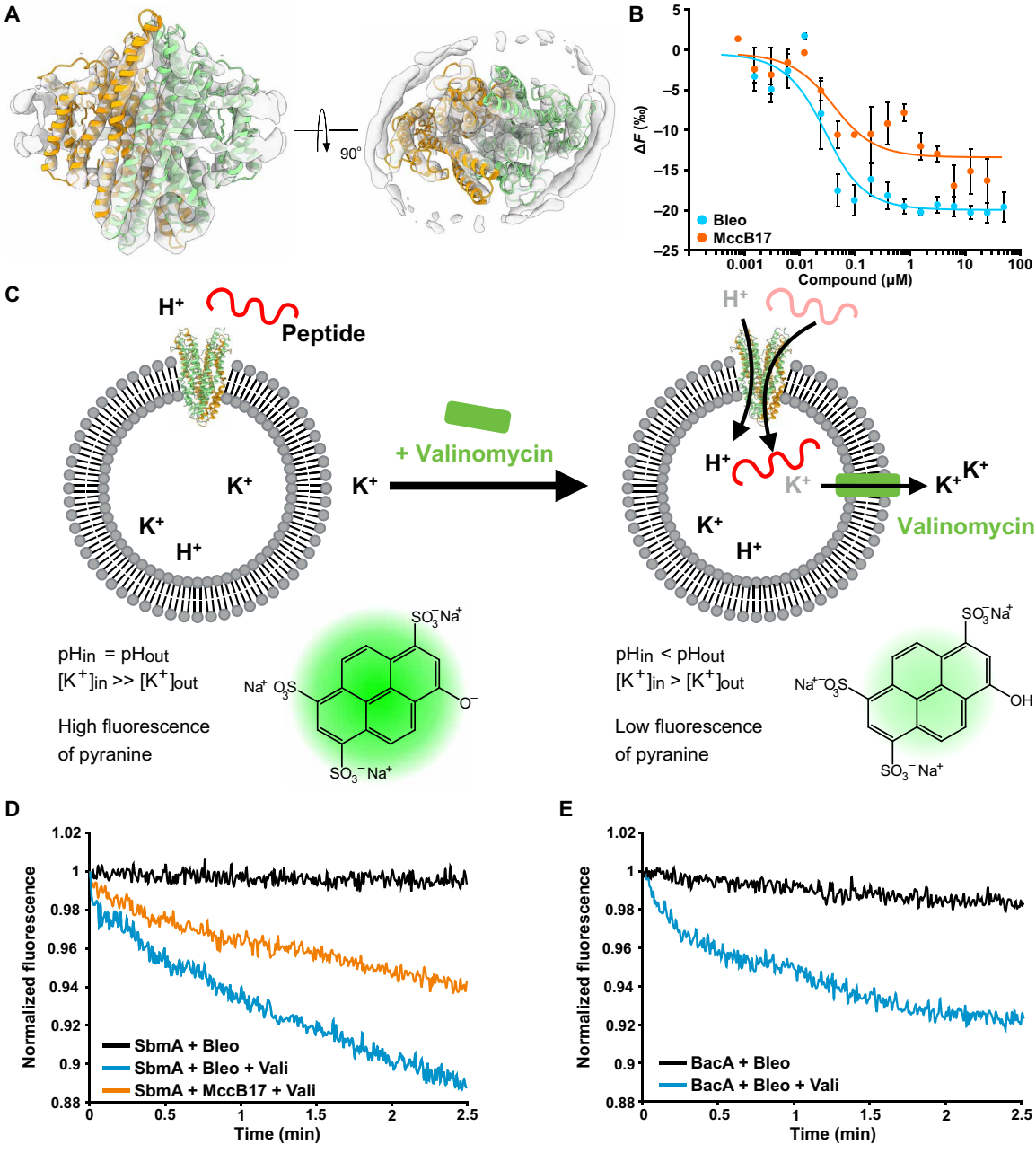

Fig. 2. Structure of BacA and functional characterization of SbmA and BacA. (**A**) Structure of SbmA fitted into the low-resolution EM map of BacA-ND showing fold conservation. (**B**). Activity of reconstituted BacA demonstrated by the binding of substrates measured by MST. (**C**) A schematic of transport assay. Addition of valinomycin creates efflux of potassium cations out of the liposome, resulting in a charge gradient across the membrane. In the presence of the substrate peptide, SbmA allows the protons to travel down the gradient, resulting in a decreased internal pH measured by pyranine fluorescence. (**D**) The transport data for SbmA in the presence of bleomycin and MccB17 show that it requires a proton gradient for substrate transport. (**E**) Transport data for BacA. BacA transport also requires a proton gradient.

We have previously shown that SbmA is a proton-driven transporter in *E. coli* cell assays (*15*). To probe the mechanism of proton translocation, we reconstituted SbmA and BacA in liposomes consisting of POPE:POPG (3:1) (fig. S9). Using the pyranine assay (Fig. 2C), we demonstrated that transport can only be initiated in the presence of both a proton gradient (induced by valinomycin) and the substrates bleomycin or MccB17 (Fig. 2, D and E, and fig. S9). Between the internal gate defined by Tyr^{368} and the cytoplasmic gate defined by Tyr^{285} and $Asp^{288'}$, the SbmA cavity is lined with conserved Glu residues, forming a "glutamate ladder," suggesting a relay path for proton movement (Fig. 3A and figs. S5 and S10). To probe their role in coordinating proton translocation, we mutated the glutamates to alanines and measured their substrate transport activity (Fig. 3B). All Glu-to-Ala mutations essentially abolished substrate transport, consistent with our previous reports. Since the transport assay only measures indirect substrate transport by monitoring pyranine

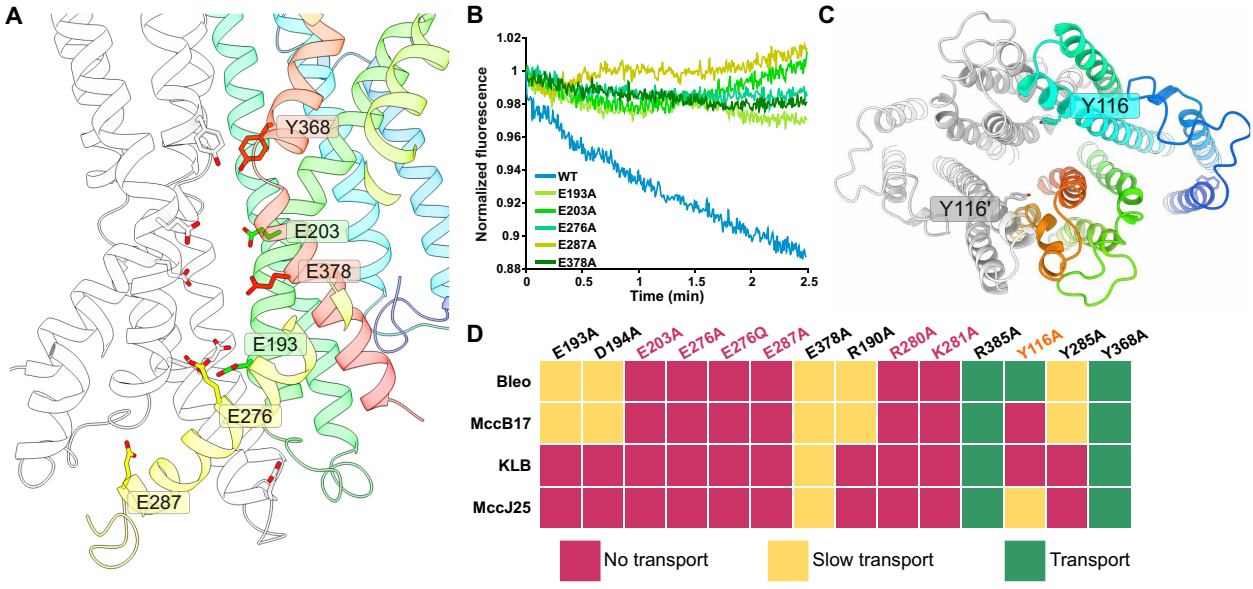

Fig. 3. Structure-functional analysis of SbmA. (**A**) A cartoon representation of SbmA and glutamates, forming the glutamate ladder. (**B**) Transport assay data for the glutamate mutants. (**C**) A cartoon representation of SbmA showing Y116 (potential periplasmic gate) residue. (**D**) Antibiotic sensitivity of SbmA mutants upon conditions of low and high expression. Green: The mutation has no effect on transport, sensitive cells. Red: Cells become fully resistant at the level of ΔSbmA strain. Yellow: Resistant phenotype under low-expression conditions and low-level sensitivity under high-expression conditions (slow transport possible).

fluorescence quenching, we performed growth inhibition and lawn-spot assays in *E. coli* Δ*sbmA* cells complemented with either wild-type (WT) SbmA or Glu mutants. We evaluated these mutants under two different conditions, low- and high-protein expression. Under low-protein expression conditions (mimicking the low abundance of protein in proteoliposomes), all the mutants made cells resistant to bleomycin, MccB17, KLB, and MccJ25 at the level of the parent Δ*sbmA* strain, providing further evidence on the role of the glutamates in proton-mediated substrate translocation (Fig. 3D and figs. S11 and S12). Under high-protein expression (preinduction of starter culture), the cells that carry the Glu^{193}Ala and Glu^{378}Ala mutants become sensitive to some antibacterial peptides, suggesting that while some proton translocation can still occur, the transporter is substantially slowed down because of either inefficient proton movement or possible disruption of required conformational changes. Thus, the high-protein expression assays allow us to distinguish between mutants with severely affected transport and those that have truly lost their transport capability. The structure and functional data suggest that the funnel-shaped central part of the TMD, as defined by TMs 6a and 6b from both protomers, can guide protons toward the glutamate ladder, which facilitates their movement.

Disruption of the second internal (Arg^{280}Ala) and cytoplasmic (Tyr^{285}Ala) gates also affects substrate transport, conferring cells with complete or almost complete resistance to all SbmA substrate antibiotics tested (Fig. 3D). Although it appears that the first internal gate, Tyr^{368}/Tyr$^{368'}$, is protecting the glutamate ladder by preventing proton dissociation, the Tyr^{368}Ala mutant not only remains sensitive to all peptides but also appears to be additionally sensitized to bleomycin, suggesting that this residue defines the boundary of the peptide-binding part of the cavity (the substrates sitting above this gate). In the absence of a peptide-bound structure, we also mutated some of the conserved arginines and lysines lining the cavity of SbmA (Lys^{281}, Arg^{190}, and Arg^{385}). Although they are forming salt bridges with the conserved glutamates, we could not exclude their role in substrate binding. All these mutants provide cells with complete or nearly complete resistance to all substrate peptides with the exception of Arg^{385} whose side chain points away from the cavity (Fig. 3D). We further hypothesized that Tyr^{116} may participate in periplasmic gate formation upon peptide transport (Fig. 3, C and D). Mutation of this residue, similar to Tyr^{368}, slightly increased sensitivity to bleomycin and notably made cells resistant to MccB17, KLB, and MccJ25. We propose that this residue might act as an anchor for initial binding of microcin peptides; in particular, in the case of MccB17 and KLB, the side chain of Tyr^{116} might stack against the azole, similar to what was observed in the case of LAPs and the ribosome (*22*). The DNA gyrase residue implicated in MccB17 binding is also an aromatic residue, GyrB Trp^{751}, suggesting a further role in MccB17 recognition (*23*). Together, this work establishes a previously unknown proton-driven secondary transporter fold as defined by the SbmA and BacA structures, which we believe should be referred to in the literature as "SbmA-like peptide transporters (SLiPT) fold" as homologs of the EcSbmA and SmBacA proteins are very likely to adopt the same overall fold.

SLiPT transporter mechanism

Our data allow us to suggest a mechanism for antibacterial peptide import by SbmA and BacA proteins (Fig. 4), reminiscent of ABC transporters. In its resting state (Fig. 4I), SbmA adopts an outward-open conformation with its cavity accessible to both peptide and proton. Binding of a proton in Glu^{203}, with subsequent movement along the glutamate ladder, and simultaneous peptide binding in the open cavity induce either a transient or a stable occluded state, similar to the ABC transporters McjD (*20*, *21*) or Rv1819c (*13*); this occluded conformation is a result of the movement of TMs 1 and 2

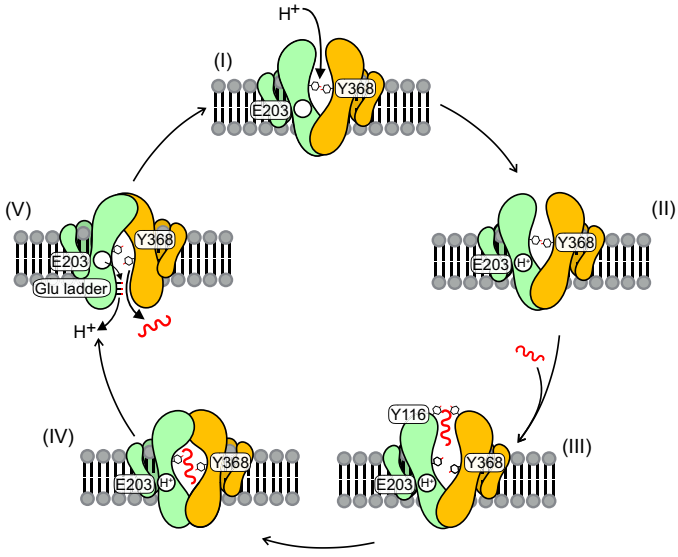

Fig. 4. Proposed mechanism for SbmA peptide transport. (I) Proton is free to bind when the transporter is in the outward-open state, but proton transport is precluded. Inner cavity is occluded by Tyr^{368}. Glu^{203} is essential for transport and is marked as a potential first proton-binding site (**II**). (**III**) Binding of substrate peptide (Tyr^{116} is essential for MccB17 and MccJ25) triggers conformational changes, resulting in a transient or stable occluded state (**IV**). (**V**) Structural rearrangements result in an inward-open conformation and subsequent release of the proton into the cytoplasm, using the glutamate ladder, leading to the dissociation of the peptide; the transporter resets in its outward-open conformation. Only one copy of the glutamate ladder and Glu^{203} is shown for clarity.

toward TMs 5′ and 6′ (Fig. 4, IV). An inward-facing open conformation can be formed by opening the cytoplasmic gate and movement of TMs 4 and 5 away from TMs 4′ and 5′; our growth assays suggest that disruption of the internal gate affects transport. Notably, all fully resistant mutants are found along TM5, suggesting its important role in substrate translocation associated with conformational changes along the transport cycle; the broken TM6, as observed in both SbmA and Rv1819c, can possibly facilitate this conformational change. In the inward-open conformation, the antibacterial peptide and proton are released in the cytoplasm, and the transporter resets in the outward-open conformation. A high degree of coupling, observed in our transport assays, suggests that proton and peptide translocation can only occur in the presence of both since they can induce the required structural rearrangements.

DISCUSSION

Although SbmA/BacA structurally resemble the TMD of ABC exporters, they are not energized by ATP as established by our functional data in proteoliposomes, growth curves, and lawn assays. We have previously shown in pull-down and bacterial two-hybrid assays the absence of any orphan NBDs that could bind to SbmA (*15*). In this study, our structures clearly demonstrate that SLiPT transporters lack the coupling helices that would be necessary for any orphan NBDs to bind and energize them (fig. S4). It has previously been shown that the ABC transporter LmrA, devoid of its NBD, can be energized by the proton gradient (*24*), although no glutamate ladder is present that could provide a clear path for proton movement. This observation, together with our structural and functional data, suggests an evolutionary link between full-length ABC transporters and SLiPTs. The possibility that the proton-driven SLiPTs may have coevolved together with or from full-length ABC transporters is further supported by the substrate promiscuity observed in SbmA and BacA transporters.

If cells can defend themselves against AMPs that kill predominantly by membrane permeabilization by importing them into the cytoplasm for degradation (e.g., *25*), the loss of the transporter sensitizes the bacteria to the peptide and reduces their virulence. Since loss of SbmA in an avian *E. coli* reduces its virulence (*8*), while loss of BacA in *B. abortus* and *S. meliloti* reduces their virulence in mouse and symbiotic proficiency, respectively, it seems likely that AMP import by SbmA/BacA may underlie its importance for interactions with eukaryotic hosts. In this logic, internalized antibiotics used in this study hijack SbmA/BacA to reach the cytoplasm. In the case of *Rhizobium*-legume symbioses, importing plant NCR peptides into the cytoplasm via BacA not only limits killing from membrane disruption (*12*) but also ensures that the NCR peptides are able to make necessary interactions with their intracellular bacterial targets to force terminal differentiation into nitrogen-fixing bacteroids. The *Rhizobium*-specific RiPP phazolicin was recently described (*22*), which is structurally similar to MccB17 and KLB. It is not known how phazolicin enters *Rhizobium* cells, but it is likely that the BacA protein would be involved. Thus, we believe that SbmA-targeting molecules provide an important avenue for the development of novel selective antibacterials that can cross the inner membrane of Gram-negative pathogens by hijacking the SbmA transporter for internalization.

MATERIALS AND METHODS

Purification of SbmA and BacA

SbmA from *E. coli* and BacA from *S. meliloti* were overexpressed in *E. coli* C43 (DE3) or Lemo21 (DE3) and purified in 20 mM tris (pH 8.0), 150 mM NaCl, and 0.03% n-Dodecyl β-D-maltoside (DDM) as previously described without modifications (fig. S1) (*15*).

Generation of anti-SbmA antibodies

All the animal experiments conformed to the guidelines of the Guide for the Care and Use of Laboratory Animals of Japan and were approved by the Kyoto University Animal Experimentation Committee. Mouse monoclonal antibodies against SbmA were raised according to the previously described method (*26*). Briefly, a proteoliposome antigen was prepared by reconstituting purified, functional SbmA at high density into phospholipid vesicles consisting of a 10:1 mixture of egg phosphatidylcholine (Avanti Polar Lipids) and the adjuvant lipid A (Sigma-Aldrich). BALB/c mice were immunized with the proteoliposome antigen using three injections at 2-week intervals. Antibody-producing hybridoma cell lines were generated using a conventional fusion protocol. Hybridoma clones producing antibodies recognizing conformational epitopes in SbmA were selected by an enzyme-linked immunosorbent assay on immobilized phospholipid vesicles containing purified SbmA, allowing positive selection of the antibodies that recognized the native conformation of SbmA. Additional screening for reduced antibody binding to SDS-denatured SbmA was used for negative selection against linear epitope–recognizing antibodies. Stable complex formation between SbmA and each antibody clone was checked using fluorescence-detection size-exclusion chromatography. The sequence of the Fab

from the antibody clone number S11-1 was determined via standard 5′-RACE using total RNA isolated from hybridoma cells.

Preparation of the SbmA-fab complex for cryo-EM

For the generation of the SbmA-Fab complex for structural studies, monoclonal antibody S11-1 was digested and purified using the Pierce Fab Preparation Kit. The purified Fab S11-1 was dialyzed in 20 mM tris (pH 7.5) including 25 mM NaCl. The SbmA and Fab S11-1 were mixed in a 1:2 molar ratio, and excess Fab was separated from the SbmA-Fab complex by size-exclusion chromatography using a Superdex S200 column (Cytiva) in 20 mM tris-Cl (pH 8.0), 150 mM NaCl, and 0.03% DDM.

ND incorporation

Plasmids for expression of MSP1D1 and MSP1E3D1 were a gift from S. Sligar (Addgene plasmid nos. 20061 and 20066) (*27*). The double cysteine mutation in MSP1E3D1 (S22C and A121C) was introduced using two steps of site-directed mutagenesis polymerase chain reactions. SLiPT discs containing SbmA and BacA were prepared as follows: Briefly, 20 μmol of desired lipid mixture was dried using gentle argon stream and subsequently placed in vacuum for at least 2 hours to remove residual chloroform. Next, the film was hydrated with 20 mM tris-Cl (pH 7.5) and 150 mM NaCl buffer and sonicated to prepare small unilamellar liposomes. Those were subsequently solubilized using DDM to yield a clear solution with a final concentration of 7.5 mM for lipids and 33 mM for DDM. Purified SbmA or BacA (7.7 to 21.3 mg ml^{-1}) was added to lipid/detergent micelles and incubated at 28°C for 30 min. Next, the membrane scaffold protein was added, followed by 5 min of incubation, addition of Amberlite XAD-2 (80 mg of damp beads per 1 mg of detergent), and overnight incubation at 28°C. The following day, the NDs were purified using Superdex 200 Increase 10/300 (Cytiva) equilibrated with cryo-EM buffer [K-Hepes 20 mM (pH 7.5) and KCl 120 mM]. The membrane protein:MSP:lipid ratios for both membrane proteins were 1:2:100 for MSP1E3D1 and 1:2:50 for MSP1D1. Lipid mixtures used for MSP1E3D1 and MSP1D1 were 13:4:1 of DOPE/POPG/POPOCL and 14:4:2 of POPE/POPG/POPOCL, respectively. The samples were then concentrated using 50-kDa centrifugal concentrators (Millipore) to a concentration of 6 to 9 mg/ml total protein and immediately used for grid preparation.

For a dataset with MccB17, purified MccB17 was added at 100 μM concentration, and the sample was incubated at 37°C for 1 hour. Fluorinated octyl maltoside, a nonsolubilizing detergent, was added at 0.05% to improve particle distribution in ice and to limit the aggregation of MccB17.

Microscale thermophoresis

For MST studies, MSP1E3D1 (S22C and A121C) was labeled using Alexa Fluor 647 C2 maleimide (Thermo Fisher Scientific). Briefly, 10 eq. of the maleimide dye dissolved in dimethyl sulfoxide (DMSO) was added to 1 eq. of MSP1E3D1 (S22C and A121C) reduced with 2 mM tris(2-carboxyethyl)phosphine (TCEP), and incubated for 2 hours at room temperature in 25 mM K-Hepes (pH 7.2) and 400 mM KCl. The labeled protein was purified from the excess dye and residual DMSO using Superdex 200 Increase 10/300 and used in the ND formation protocol described above. The labeling efficiency was measured by the 280- and 650-nm absorbance of the final protein product, and the typical yield was in the range of 1.65- to 1.8-labeled cysteines per MSP1E3D1 (S22C and A121C).

MST experiments were performed using a Monolith NT.115 (NanoTemper) instrument using a red filter set. SbmA-containing Alexa Fluor 647–labeled NDs [20 nM in 20 mM K-Hepes (pH 8) and 150 mM KCl] were mixed with bleomycin, KLB, and MccB17 (the last two were dissolved in DMSO; the final DMSO concentration in the reaction was 1.25%) and incubated in MST buffer [20 mM K-Hepes (pH 8), 150 mM KCl, and 0.005% Tween 20] in the dark for 15 min.

Fluorescence signal was measured using MO.Control software (Nanotemper) in Monolith NT.115 Premium Capillaries (#MO-K025). MST signal was used for binding analysis in MO.Affinity software (Nanotemper) using 1:1 binding mode. The K_d values were calculated on the basis of three independent measurements. All experiments were performed at room temperature.

Electron microscopy

Aliquots of 4 μl of ND-embedded complexes (~3 to 5 mg/ml) were applied to glow-discharged Quantifoil holey carbon grids (R1.2/1.3, 300 mesh). After 30 s of incubation with 95% chamber humidity at 10°C, the grids were blotted for 6 s and plunge-frozen in liquid ethane using a Vitrobot mark IV (FEI).

Cryo-EM data were collected at the Polish national cryo-EM facility SOLARIS or eBIC (DLS, UK for BacA-free dataset) with a Titan Krios G3i microscope (Thermo Fisher Scientific) operated at 300 kV, and images were collected at a nominal magnification of ×105,000 resulting in a calibrated physical pixel size of 0.86 Å per pixel with a defocus range of −3 to −0.9 μm. The images were recorded in counting mode on a K3 electron direct detector (Gatan) equipped with GIF BIO Quantum energy filter operated with a slit width of 20 eV. A dose rate of 15 electrons per pixel per second was used, and exposure time was set to generate a total dose of ~40 electrons/$Å^2$ over 40 movie frames. Statistics for cryo-EM data collection are listed in table S1.

Data processing

For the SbmA-Fab dataset, 5421 movies were imported to cryoSPARC v2.15 for patch motion and contrast transfer function (CTF) correction (*28*). A total of 2000 particles were manually picked to train a Topaz model (*29*), used initially to pick 100 micrographs. Another round of Topaz training was performed, using cleaned-up particles from this small subset. This improved model was applied to the whole dataset, yielding 1,236,218 particles. After rounds of 2D classification in cryoSPARC, an initial model was produced with a global resolution of ~4.2 Å. This model was used to create templates used for particle picking during the final round of processing (fig. S3). In this final round, template-picking resulted in 1,182,621 particles, which were extracted with a pixel size of 1.72 Å per pixel and cleaned up in multiple rounds of 2D classification. Ab initio procedure in cryoSPARC was used for further cleaning of particle stack. Iterative rounds of cryoSPARC nonuniform refinement (*30*) with C2 symmetry imposed, followed by reextraction of full-size particles, local motion (*31*), and CTF correction (*32*), yielded a final map with a global resolution of 3.74 Å from 320,796 particles. For the processing of SbmA-Fab-MccB17 data, initial analysis using Topaz-picked particles showed that the structures are indistinguishable from SbmA-Fab. Therefore, templates from the latter model were used for picking, resulting in 407,426 particles from 7286 micrographs. After particle cleaning by 2D classification and ab initio 3D classification, particles were reextracted; local motion and CTF correction were performed, resulting

in a final 3.59-Å map from 116,545 particles after cryoSPARC nonuniform refinement. The local resolution for SbmA protein was estimated by cryoSPARC to lie between 3.1 and 3.4 Å. This map was postprocessed by DeepEMhancer (*33*), which further improved connectivity and was used for model building and refinement.

SbmA without Fabs dataset was processed in a similar way (fig. S7). Templates were prepared after initial Topaz picking, and template-based picking of 6881 micrographs resulted in 2,060,359 particles. The 2 × 2 binned particles (1.72 Å per pixel) were subjected to multiple rounds of 2D classification in cryoSPARC to remove empty NDs and contamination classes. The resulting stack of 298,548 particles was used to produce ab initio model in cryoSPARC; however, ab initio classification failed to separate high-resolution particles. Therefore, particles were imported to RELION 3.1 (*34*) using pyem script (*35*) and subjected to unsupervised 3D classification with no symmetry imposed and soft mask over the whole particle. One of four classes (63,291 particles) was found to display clear transmembrane helices; this class was imported back to cryoSPARC, and after extraction of full-size (0.86 Å per pixel) particles, subjected to nonuniform refinement with local CTF correction. The final map derived from 62,372 particles had a global resolution of 4.06 Å as estimated by cryoSPARC.

For the BacA-free dataset, 405,208 particles were picked from 2980 micrographs using the Topaz model trained on a small manually picked subset. After multiple rounds of cryoSPARC 2D classification, class averages with clear protein features (105,059 particles) were selected. Ab initio classification showed that two populations of NDs are present, one being slightly larger than the other (~100 and ~110 Å diameter). Both subsets of particles were imported to RELION 3.1 and subjected to unsupervised 3D classification. For the final reported map, 17,648 particles with clear density for TM helices were selected from a small ND class and imported back to cryoSPARC v3.2 for non-uniform refinement with adaptive marginalization, resulting in a global resolution of 6.36 Å as estimated by cryoSPARC.

SbmA model building and refinement

In the absence of a suitable homologous structure, we built the de novo structure of SbmA. An initial model was generated by Buccaneer under the collaborative computational project for electron cryomicroscopy (CCP-EM) suite using C2 symmetry and further refined in Phenix using real-space refinement (*36*). Most of the helices and side chains were placed within the density. Further manual building with addition of missing residues was performed in Coot (*37*) with secondary structure restraints to constrain the geometry of the helices. The ~3.2-Å resolution of the SbmA allowed us to build all missing helices and to also correct the register of the Buccaneer model and generate a final structure that comprises residues 1 to 391; there was no density to build the last 15 residues. Clear density for a PG molecule was also present and was manually placed in Coot. Further improvement of the overall geometry was facilitated by ISOLDE (*38*) in ChimeraX (*39*). Since the local resolution for the Fab S11-1 was worse than 6 Å, we could not build its de novo structure or refine it. The closest structural homolog to Fab S11-1 is the antitumor antibody A5B7 with Protein Data Bank (PDB) ID 1CLO (*40*); most sequence differences are at the complementarity-determining region loops. The sequence of the Fab S11-1 was matched onto the A5B7 and placed by molecular replacement using Molrep (*41*) under the CCP-EM suite (*42*, *43*). The placed Fab was then rigid-body refined. The final SbmA model was refined with C2 symmetry in Phenix using real-space refinement (*36*). The Ramachandran plot does not show any outliers. The model refinement and validation statistics are shown in table S1.

Model validation

The structural model of SbmA protein was validated using MolProbity (*44*). Cross-validation to check the possibility of overfitting and the predictive power of the model was performed using a half-map validation approach (*45*). Briefly, the atom positions of the final model were randomly displaced by 0.5 Å. Then, refinement against half of data from the final map reconstruction is performed using the same parameters used to obtain the final model. An EM map was created from the refined model using ChimeraX molmap plugin, with the Fourier shell correlation (FSC) = 0.143 resolution (3.6 Å) as a filtering threshold. The FSC was then calculated for both the half-map against which it had been refined and the map from the other half of the data, up to a resolution of 2 Å (FSCwork and FSCtest). Significant correlation was observed (*t* test for Pearson correlation $r = 0.79$ $P = 4.99 \times 10^{-5}$) beyond the resolution used for refinement up to 3 Å, demonstrating predictive power for the model and absence of over-fitting.

Transport assay

SbmA and BacA proteins for functional assays were reconstituted in liposomes using the rapid dilution method. POPE/POPG lipids (Avanti Polar Lipids) were mixed in a 3:1 ratio, and chloroform was removed by nitrogen gas. The POPE/POPG mixture forms tight liposomes without proton leakage. The dried lipid film was resuspended in MilliQ water in a final concentration of 20 mg/ml and sonicated in a water bath until the solution became less hazy. The liposomes were destabilized by the addition of 1.0% DDM. SbmA WT, glutamate mutants (E193A, E203A, E276A, E287A, and E378A), and BacA (1.0 mg/ml) were mixed in a 1:4 ratio (protein:lipid) with 300 µl of lipid vesicles and were incubated on ice for 30 min. The protein-liposome mixture was rapidly diluted into 60 ml of reconstitution buffer [5 mM K-Hepes (pH 6.8), 120 mM KCl, and 2 mM $MgSO_4$], and proteoliposomes were harvested by ultracentrifugation (~200,000*g*) for 2 hours. The pelleted liposomes were resuspended in reconstitution buffer, and their concentration was determined using a bicinchoninic acid (BCA) kit (Pierce) and dialyzed against 2 liters of reconstitution buffer overnight to remove any remaining detergent. Reconstitution efficiency was also determined by analyzing the proteoliposomes by SDS–polyacrylamide gel electrophoresis (fig. S9).

The proteoliposomes were subjected to three rounds of freeze-thaw in liquid nitrogen and harvested by ultracentrifugation (100,000*g*) for 30 min. The pelleted proteoliposomes were resuspended in inside buffer [5 mM K-Hepes (pH 6.8), 1 mM pyranine (trisodium 8-hydroxypyrene-1,3,6-trisulfonate), 120 mM KCl, and 2 mM $MgSO_4$] and subjected to three rounds of freeze-thaw in liquid nitrogen. The proteoliposomes were harvested by ultracentrifugation (100,000*g*) for 30 min, and the pellets were washed to remove any free pyranine and resuspended in reconstitution buffer. For the transport assay, liposomes at a final concentration of 15 µM were placed in a cuvette and quickly mixed with 1.0 ml of outside buffer [5 mM K-Hepes (pH 6.8), 1.2 mM KCl, and 2 mM $MgSO_4$] containing bleomycin (100 µM) or MccB17 (30 µM) with or without valinomycin (1 µM). To assess that the proteoliposomes are tight and do not leak protons, liposomes were mixed with 1 ml of low pH buffer [10 mM

MES-Cl (pH 6.0) and 1.2 mM KCl], and their fluorescence was measured; no apparent change was detectable. Data were recorded using a Cary Eclipse Fluorescence Spectrophotometer (Agilent Technologies) at the following settings: 460-nm excitation, 510-nm emission, 5-nm slit width, and 0.5-s resolution for 2.5 min. The fluorescent data have been normalized to allow direct comparison. Transport assays were measured in triplicate.

Construction of SbmA mutants

Full-length *sbmA* (1-406) from *E. coli* K12 MG1655 was cloned into pBAD A Myc-His vector that carries a C-terminal His6-tag (Thermo Fisher Scientific) and expressed in strain JW0368-1 [F-, Δ(araD-araB)567, ΔlacZ4787(::rrnB-3), ΔsbmA742::kan, λ-, rph-1, Δ(rhaD-rhaB)568, hsdR514] (a parent strain of Keio knockout collection). SbmA mutants were generated using the QuikChange Site-Directed Mutagenesis Kit (Agilent Technologies); DNA sequencing confirmed the presence of the mutations. To confirm that the WT protein and mutants express at similar levels during the growth inhibition assays, we estimated their expression by Western blot. The cells were incubated in LB medium–supplemented kanamycin (50 μg/ml) and ampicillin (100 μg/ml); when the cultures reached an optical density (OD_{600}) = 0.6, arabinose was added at the final concentration of 0.0002% and incubated at 37°C for further 2.5 hours. Membranes were isolated by breaking the cells with 0.1-mm glass beads. After ultracentrifugation, the pelleted membranes were resuspended in phosphate-buffered saline buffer, and the expression was confirmed by anti-His antibody Western blot. All proteins expressed at similar levels (fig. S13).

Growth inhibition assays

Growth curves were measured to analyze the ability of SbmA mutants to transport bleomycin. Overnight cultures of *E. coli* strain JW0368 (Δ*sbmA*::KmR) from the Keio collection transformed with expression plasmids for SbmA mutants were grown in LB medium supplemented with kanamycin (30 μg/ml) and ampicillin (100 μg/ml). The growth assay was carried out in 200-μl volumes using sterile, flat-bottomed 96-well plates (Thermo Fisher Scientific). LB medium was supplemented with kanamycin (30 μg/ml), ampicillin (100 μg/ml), 10 μM L-arabinose, and 5 μM bleomycin sulfate (Sigma-Aldrich) and inoculated with overnight culture in a ratio of 1:100. Control experiments contained no bleomycin sulfate. Cells were grown at 37°C with shaking in a SpectraMAX190 (Molecular Devices) plate reader. The OD_{600} was measured every minute for 17 hours. Measurements were carried out in technical triplicates from three independent clones (biological replicas).

Spot-on-lawn assays

The activity of KLB, MccJ25, or MccB17 against strains expressing SbmA mutants was evaluated using a "spot on lawn" technique. M9 [M9 salts with 1% glycerol and thiamine (10 μg/ml)] or LB 1% agar was supplemented with ampicillin (100 μg/ml) and 10 μM arabinose and prepared in 9-cm aseptic petri dishes (VWR). Overnight cultures of *E. coli* strain JW0368 (Δ*sbmA*::KmR) transformed with expression plasmids for SbmA mutants, growing in an appropriate medium, were diluted in a ratio of 1:40 (adjusted according to the final culture OD, if necessary) in liquid 0.6% agar, which was overlaid onto the M9 or LB agar plates. Two microliters of each inhibitor dilution (KLB, 500 μM; MccB17 and MccJ25, 100 μM) was spotted onto the surface of the seeded agar. Plates were incubated for 30 hours at 30°C (M9) or overnight at 37°C (LB).

SUPPLEMENTARY MATERIALS

Supplementary material for this article is available at https://science.org/doi/10.1126/sciadv.eabj5363

View/request a protocol for this paper from *Bio-protocol*.

REFERENCES AND NOTES

1. M. Lavina, A. P. Pugsley, F. Moreno, Identification, mapping, cloning and characterization of a gene (*sbmA*) required for microcin B17 action on *Escherichia coli* K12. *J. Gen. Microbiol.* **132**, 1685–1693 (1986).
2. R. A. Salomon, R. N. Farias, The peptide antibiotic microcin 25 is imported through the TonB pathway and the SbmA protein. *J. Bacteriol.* **177**, 3323–3325 (1995).
3. M. Metelev, I. A. Osterman, D. Ghilarov, N. F. Khabibullina, A. Yakimov, K. Shabalin, I. Utkina, D. Y. Travin, E. S. Komarova, M. Serebryakova, T. Artamonova, M. Khodorkovskii, A. L. Konevega, P. V. Sergiev, K. Severinov, Y. S. Polikanov, Klebsazolicin inhibits 70S ribosome by obstructing the peptide exit tunnel. *Nat. Chem. Biol.* **13**, 1129–1136 (2017).
4. P. Yorgey, J. Lee, J. Kordel, E. Vivas, P. Warner, D. Jebaratnam, R. Kolter, Posttranslational modifications in microcin B17 define an additional class of DNA gyrase inhibitor. *Proc. Natl. Acad. Sci. U.S.A.* **91**, 4519–4523 (1994).
5. M. Mattiuzzo, A. Bandiera, R. Gennaro, M. Benincasa, S. Pacor, N. Antcheva, M. Scocchi, Role of the *Escherichia coli* SbmA in the antimicrobial activity of proline-rich peptides. *Mol. Microbiol.* **66**, 151–163 (2007).
6. S. E. Puckett, K. A. Reese, G. M. Mitev, V. Mullen, R. C. Johnson, K. R. Pomraning, B. L. Mellbye, L. D. Tilley, P. L. Iversen, M. Freitag, B. L. Geller, Bacterial resistance to antisense peptide phosphorodiamidate morpholino oligomers. *Antimicrob. Agents Chemother.* **56**, 6147–6153 (2012).
7. A. Ghosal, A. Vitali, J. E. Stach, P. E. Nielsen, Role of SbmA in the uptake of peptide nucleic acid (PNA)-peptide conjugates in *E. coli*. *ACS Chem. Biol.* **8**, 360–367 (2013).
8. G. Li, C. Laturnus, C. Ewers, L. H. Wieler, Identification of genes required for avian *Escherichia coli* septicemia by signature-tagged mutagenesis. *Infect. Immun.* **73**, 2818–2827 (2005).
9. K. LeVier, R. W. Phillips, V. K. Grippe, R. M. Roop II, G. C. Walker, Similar requirements of a plant symbiont and a mammalian pathogen for prolonged intracellular survival. *Science* **287**, 2492–2493 (2000).
10. J. Glazebrook, A. Ichige, G. C. Walker, A Rhizobium meliloti homolog of the *Escherichia coli* peptide-antibiotic transport protein SbmA is essential for bacteroid development. *Genes Dev.* **7**, 1485–1497 (1993).
11. A. Ichige, G. C. Walker, Genetic analysis of the Rhizobium meliloti bacA gene: Functional interchangeability with the Escherichia coli sbmA gene and phenotypes of mutants. *J. Bacteriol.* **179**, 209–216 (1997).
12. A. F. Haag, M. Baloban, M. Sani, B. Kerscher, O. Pierre, A. Farkas, R. Longhi, E. Boncompagni, D. Hérouart, S. Dall'Angelo, E. Kondorosi, M. Zanda, P. Mergaert, G. P. Ferguson, Protection of *Sinorhizobium* against host cysteine-rich antimicrobial peptides is critical for symbiosis. *PLOS Biol.* **9**, e1001169 (2011).
13. S. Rempel, C. Gati, M. Nijland, C. Thangaratnarajah, A. Karyolaimos, J. W. de Gier, A. Guskov, D. J. Slotboom, A mycobacterial ABC transporter mediates the uptake of hydrophilic compounds. *Nature* **580**, 409–412 (2020).
14. M. F. F. Arnold, A. F. Haag, S. Capewell, H. I. Boshoff, E. K. James, R. McDonald, I. Mair, A. M. Mitchell, B. Kerscher, T. J. Mitchell, P. Mergaert, C. E. Barry III, M. Scocchi, M. Zanda, D. J. Campopiano, G. P. Ferguson, Partial complementation of *Sinorhizobium meliloti bacA* mutant phenotypes by the *Mycobacterium tuberculosis* BacA protein. *J. Bacteriol.* **195**, 389–398 (2013).
15. G. Runti, M. C. Lopez Ruiz, T. Stoilova, R. Hussain, M. Jennions, H. G. Choudhury, M. Benincasa, R. Gennaro, K. Beis, M. Scocchi, Functional characterization of SbmA, a bacterial inner membrane transporter required for importing the antimicrobial peptide Bac7(1-35). *J. Bacteriol.* **195**, 5343–5351 (2013).
16. A. Ward, C. L. Reyes, J. Yu, C. B. Roth, G. Chang, Flexibility in the ABC transporter MsbA: Alternating access with a twist. *Proc. Natl. Acad. Sci. U.S.A.* **104**, 19005–19010 (2007).
17. R. J. Dawson, K. P. Locher, Structure of a bacterial multidrug ABC transporter. *Nature* **443**, 180–185 (2006).
18. S. Mehmood, V. Corradi, H. G. Choudhury, R. Hussain, P. Becker, D. Axford, S. Zirah, S. Rebuffat, D. P. Tieleman, C. V. Robinson, K. Beis, Structural and functional basis for lipid synergy on the activity of the antibacterial peptide ABC Transporter McjD. *J. Biol. Chem.* **291**, 21656–21668 (2016).
19. H. Krishnamurthy, E. Gouaux, X-ray structures of LeuT in substrate-free outward-open and apo inward-open states. *Nature* **481**, 469–474 (2012).
20. H. G. Choudhury, Z. Tong, I. Mathavan, Y. Li, S. Iwata, S. Zirah, S. Rebuffat, H. W. van Veen, K. Beis, Structure of an antibacterial peptide ATP-binding cassette transporter in a novel outward occluded state. *Proc. Natl. Acad. Sci. U.S.A.* **111**, 9145–9150 (2014).
21. K. Bountra, G. Hagelueken, H. G. Choudhury, V. Corradi, K. el Omari, A. Wagner, I. Mathavan, S. Zirah, W. Yuan Wahlgren, D. P. Tieleman, O. Schiemann, S. Rebuffat, K. Beis,

Structural basis for antibacterial peptide self-immunity by the bacterial ABC transporter McjD. *EMBO J.* **36**, 3062–3079 (2017).
22. D. Y. Travin, Z. L. Watson, M. Metelev, F. R. Ward, I. A. Osterman, I. M. Khven, N. F. Khabibullina, M. Serebryakova, P. Mergaert, Y. S. Polikanov, J. H. D. Cate, K. Severinov, Structure of ribosome-bound azole-modified peptide phazolicin rationalizes its species-specific mode of bacterial translation inhibition. *Nat. Commun.* **10**, 4563 (2019).
23. J. L. Vizán, C. Hernández-Chico, I. del Castillo, F. Moreno, The peptide antibiotic microcin B17 induces double-strand cleavage of DNA mediated by E. coli DNA gyrase. *EMBO J.* **10**, 467–476 (1991).
24. H. Venter, R. A. Shilling, S. Velamakanni, L. Balakrishnan, H. W. van Veen, An ABC transporter with a secondary-active multidrug translocator domain. *Nature* **426**, 866–870 (2003).
25. C. L. Shelton, F. K. Raffel, W. L. Beatty, S. M. Johnson, K. M. Mason, Sap transporter mediated import and subsequent degradation of antimicrobial peptides in *Haemophilus*. *PLOS Pathog.* **7**, e1002360 (2011).
26. F. Jaenecke, Y. Nakada-Nakura, K. Nagarathinam, S. Ogasawara, K. Liu, Y. Hotta, S. Iwata, N. Nomura, M. Tanabe, Generation of conformation-specific antibody fragments for crystallization of the multidrug resistance transporter MdfA. *Methods Mol. Biol.* **1700**, 97–109 (2018).
27. I. G. Denisov, Y. V. Grinkova, A. A. Lazarides, S. G. Sligar, Directed self-assembly of monodisperse phospholipid bilayer Nanodiscs with controlled size. *J. Am. Chem. Soc.* **126**, 3477–3487 (2004).
28. A. Punjani, J. L. Rubinstein, D. J. Fleet, M. A. Brubaker, cryoSPARC: algorithms for rapid unsupervised cryo-EM structure determination. *Nat. Methods* **14**, 290–296 (2017).
29. T. Bepler, A. Morin, M. Rapp, J. Brasch, L. Shapiro, A. J. Noble, B. Berger, Positive-unlabeled convolutional neural networks for particle picking in cryo-electron micrographs. *Nat. Methods* **16**, 1153–1160 (2019).
30. A. Punjani, H. Zhang, D. J. Fleet, Non-uniform refinement: Adaptive regularization improves single-particle cryo-EM reconstruction. *Nat. Methods* **17**, 1214–1221 (2020).
31. J. L. Rubinstein, M. A. Brubaker, Alignment of cryo-EM movies of individual particles by optimization of image translations. *J. Struct. Biol.* **192**, 188–195 (2015).
32. J. Zivanov, T. Nakane, S. H. W. Scheres, Estimation of high-order aberrations and anisotropic magnification from cryo-EM data sets in RELION-3.1. *IUCrJ* **7**, 253–267 (2020).
33. R. Sanchez-Garcia, J. Gomez-Blanco, A. Cuervo, J. M. Carazo, C. O. S. Sorzano, J. Vargas, DeepEMhancer: A deep learning solution for cryo-EM volume post-processing. *bioRxiv* 2020.06.12.148296 (2020).
34. S. H. Scheres, A Bayesian view on cryo-EM structure determination. *J. Mol. Biol.* **415**, 406–418 (2012).
35. D. Asarnow, E. Palovcak, Y. Cheng, asarnow/pyem: UCSF pyem v0.5 (Version v0.5) *Zenodo* (2019).
36. P. V. Afonine, B. K. Poon, R. J. Read, O. V. Sobolev, T. C. Terwilliger, A. Urzhumtsev, P. D. Adams, Real-space refinement in *PHENIX* for cryo-EM and crystallography. *Acta Crystallogr. Sec. D Struct. Biol.* **74**, 531–544 (2018).
37. P. Emsley, K. Cowtan, *Coot*: Model-building tools for molecular graphics. *Acta Crystallogr. Sec. D Struct. Biol.* **60**, 2126–2132 (2004).
38. T. I. Croll, *ISOLDE*: A physically realistic environment for model building into low-resolution electron-density maps. *Acta Crystallogr. Sec. D Struct. Biol.* **74**, 519–530 (2018).
39. E. F. Pettersen, T. D. Goddard, C. C. Huang, E. C. Meng, G. S. Couch, T. I. Croll, J. H. Morris, T. E. Ferrin, UCSF ChimeraX: Structure visualization for researchers, educators, and developers. *Protein Sci.* **30**, 70–82 (2021).
40. M. J. Banfield, D. J. King, A. Mountain, R. L. Brady, V_L:V_H domain rotations in engineered antibodies: Crystal structures of the Fab fragments from two murine antitumor antibodies and their engineered human constructs. *Proteins* **29**, 161–171 (1997).
41. A. Vagin, A. Teplyakov, *MOLREP*: An automated program for molecular replacement. *J. Appl. Cryst.* **30**, 1022–1025 (1997).
42. C. Wood, T. Burnley, A. Patwardhan, S. Scheres, M. Topf, A. Roseman, M. Winn, Collaborative computational project for electron cryo-microscopy. *Acta Crystallogr. Sec. D Struct. Biol.* **71**, 123–126 (2015).
43. T. Burnley, C. M. Palmer, M. Winn, Recent developments in the *CCP-EM* software suite. *Acta Crystallogr. Sec. D Struct. Biol.* **73**, 469–477 (2017).
44. V. B. Chen, W. B. Arendall III, J. J. Headd, D. A. Keedy, R. M. Immormino, G. J. Kapral, L. W. Murray, J. S. Richardson, D. C. Richardson, MolProbity: All-atom structure validation for macromolecular crystallography. *Acta Crystallogr. D Biol. Crystallogr.* **66**, 12–21 (2010).
45. A. Amunts, A. Brown, X. C. Bai, J. L. Llacer, T. Hussain, P. Emsley, F. Long, G. Murshudov, S. H. W. Scheres, V. Ramakrishnan, Structure of the yeast mitochondrial large ribosomal subunit. *Science* **343**, 1485–1489 (2014).
46. H. Ashkenazy, S. Abadi, E. Martz, O. Chay, I. Mayrose, T. Pupko, N. Ben-Tal, ConSurf 2016: An improved methodology to estimate and visualize evolutionary conservation in macromolecules. *Nucleic Acids Res.* **44**, W344–W350 (2016).
47. M. Landau, I. Mayrose, Y. Rosenberg, F. Glaser, E. Martz, T. Pupko, N. Ben-Tal, ConSurf 2005: The projection of evolutionary conservation scores of residues on protein structures. *Nucleic Acids Res.* **33**, W299–W302 (2005).
48. A. M. Waterhouse, J. B. Procter, D. M. Martin, M. Clamp, G. J. Barton, Jalview Version 2—A multiple sequence alignment editor and analysis workbench. *Bioinformatics* **25**, 1189–1191 (2009).
49. J. D. Thompson, T. J. Gibson, F. Plewniak, F. Jeanmougin, D. G. Higgins, The CLUSTAL_X windows interface: Flexible strategies for multiple sequence alignment aided by quality analysis tools. *Nucleic Acids Res.* **25**, 4876–4882 (1997).

Acknowledgments: We thank the cryo-EM facility and staff at the SOLARIS National Synchrotron Radiation Centre, Poland. We thank M. Rawski and P. Indyka for the excellent technical support during the data collection. We acknowledge MCB Structural Biology Core Facility (supported by the TEAM TECH CORE FACILITY/2017-4/6 grant from the Foundation for Polish Science). We also thank Diamond Light Source for access and support of the cryo-EM facilities at the U.K. National Electron Bio-Imaging Centre (eBIC), proposal EM18659, funded by the Wellcome Trust, MRC, and BBSRC. The cryo-EM data analysis was supported by the PLGrid infrastructure. KLB was donated by D. Travin (Skolkovo Institute of Science and Technology; Moscow, Russia). The cryo-EM model validation plot was prepared by L. Mazurek. S. Świątek provided help with MSP1E3D1 protein purification. We would also like to acknowledge M. Towrie (STFC) for providing access to the Cary Eclipse Fluorescence Spectrophotometer.
Funding: Funding for this work was provided by Biotechnology and Biological Sciences Research Council grant BB/H01778X/1 (K.B.), Team program of the Foundation for Polish Science cofinanced by the European Union under the European Regional Development Fund TEAM/2016-3/23 (J.G.H. and P.S.), National Science Centre (NCN, Poland) grant nos. 2016/21/B/CC1/00274 (OPUS 11) (Z.P., D.G., and J.G.H.) and 2019/35/D/NZ1/01770 (SONATA 15) (Z.P., E.M., and D.G.), the Chinese Scholarship Council Scheme (F.Q.), the Japan Society for the Promotion of Science Overseas Fellowship (S.I.-I.), Basis for Supporting Innovative Drug Discovery and Life Science Research (BINDS) from the Japan Agency of Medical Research and Development (AMED) (grant no. 20am0101079) and from Research on Development of New Drugs from the AMED (S.I.), and National Institutes of Health (NIH) grant GM31030 (G.C.W.). G.C.W. is an American Cancer Society professor. The open-access publication of this article was funded by the BioS Priority Research Area under the program "Excellence Initiative – Research University" at the Jagiellonian University in Krakow. **Author contributions:** K.B. designed and managed the project. J.G.H. oversaw work carried out at Malopolska Centre of Biotechnology. D.G. collected and analyzed cryo-EM data. S.I.-I. and F.Q. prepared proteins and antibodies for cryo-EM analysis. S.I.-I. performed cloning and mutagenesis, purified proteins for binding assays, and performed proteoliposome transport assays. P.S. performed mutagenesis, purification, and labeling of MSP proteins. Z.P. measured binding affinities by MST and assisted with figures preparation. E.M. and D.G. performed growth inhibition assays. E.M. purified MccB17 and KLB peptides. K.B. and S.I.-I. built and refined the model. N.N., S.O., and S.I. screened and produced anti-SbmA antibodies. S.R. provided the MccJ25 peptide. G.W. helped with data analysis. K.B. wrote the manuscript with input from all the authors.
Competing interests: The authors declare that they have no competing interests. **Data and materials availability:** All data needed to evaluate the conclusions in the paper are present in the paper and/or the Supplementary Materials. The SbmA coordinates have been submitted to the Protein Data Bank (https://www.rcsb.org/) with PDB ID 7P34. Final EM maps of SbmA-FabS11-1-ND, SbmA-ND, and BacA-ND have been submitted to Electron Microscopy Data Bank (https://www.ebi.ac.uk/pdbe/emdb/) with IDs EMD-13168, EMD-13173, and EMD131-75, respectively. Raw data for SbmA-FabS11-1-ND and SbmA-ND were submitted to Electron Microscopy Public Image Archive (https://www.ebi.ac.uk/pdbe/emdb/empiar/) with IDs EMPIAR-10777 and EMPIAR-10763, respectively.

Submitted 19 May 2021
Accepted 16 July 2021
Published 8 September 2021
10.1126/sciadv.abj5363

Citation: D. Ghilarov, S. Inaba-Inoue, P. Stepien, F. Qu, E. Michalczyk, Z. Pakosz, N. Nomura, S. Ogasawara, G. C. Walker, S. Rebuffat, S. Iwata, J. G. Heddle, K. Beis, Molecular mechanism of SbmA, a promiscuous transporter exploited by antimicrobial peptides. *Sci. Adv.* **7**, eabj5363 (2021).

ScienceAdvances

Molecular mechanism of SbmA, a promiscuous transporter exploited by antimicrobial peptides

Dmitry GhilarovSatomi Inaba-InouePiotr StepienFeng QuElizabeth MichalczykZuzanna PakoszNorimichi NomuraSatoshi OgasawaraGraham Charles WalkerSylvie RebuffatSo IwataJonathan Gardiner HeddleKonstantinos Beis

Sci. Adv., 7 (37), eabj5363. • DOI: 10.1126/sciadv.abj5363